9-2009

Differential Inhibition of Various Adenylyl Cyclase Isoforms and Soluble Guanylyl Cyclase by 2',3'-O-(2,4,6-Trinitrophenyl)-Substituted Nucleoside 5'-Triphosphates

Srividya Suryanarayana

Martin Göttle

Melanie Hübner

Andreas Gille

Tung-Chung Mou

See next page for additional authors

0022-3565/09/3303-687–695$20.00
THE JOURNAL OF PHARMACOLOGY AND EXPERIMENTAL THERAPEUTICS
JPET 330:687–695, 2009

Vol. 330, No. 3
155432/3501184
Printed in U.S.A.

Differential Inhibition of Various Adenylyl Cyclase Isoforms and Soluble Guanylyl Cyclase by 2′,3′-*O*-(2,4,6-Trinitrophenyl)-Substituted Nucleoside 5′-Triphosphates

Srividya Suryanarayana,[1] Martin Göttle, Melanie Hübner, Andreas Gille,[2] Tung-Chung Mou, Stephen R. Sprang, Mark Richter, and Roland Seifert

Department of Molecular Biosciences (S.S., M.R.) and Department of Pharmacology and Toxicology (A.G.), the University of Kansas, Lawrence, Kansas; Department of Pharmacology and Toxicology, University of Regensburg, Regensburg, Germany (M.G., M.H.); Center for Biomolecular Structure and Dynamics, University of Montana, Missoula, Montana (T.-C.M., S.R.S.); and Institute of Pharmacology, Medical School of Hannover, Hannover, Germany (R.S.)

Received April 22, 2009; accepted June 2, 2009

ABSTRACT

Adenylyl cyclases (ACs) catalyze the conversion of ATP into the second messenger cAMP and play a key role in signal transduction. In a recent study (*Mol Pharmacol* **70:**878–886, 2006), we reported that 2′,3′-*O*-(2,4,6-trinitrophenyl)-substituted nucleoside 5′-triphosphates (TNP-NTPs) are potent inhibitors (K_i values in the 10 nM range) of the purified catalytic subunits VC1 and IIC2 of membranous AC (mAC). The crystal structure of VC1:IIC2 in complex with TNP-ATP revealed that the nucleotide binds to the catalytic site with the TNP-group projecting into a hydrophobic pocket. The aims of this study were to analyze the interaction of TNP-nucleotides with VC1:IIC2 by fluorescence spectroscopy and to analyze inhibition of mAC isoforms, soluble AC (sAC), soluble guanylyl cyclase (sGC), and G-proteins by TNP-nucleotides. Interaction of VC1:IIC2 with TNP-NDPs and TNP-NTPs resulted in large fluorescence increases that were differentially reduced by a water-soluble forskolin analog. TNP-ATP turned out to be the most potent inhibitor for ACV (K_i, 3.7 nM) and sGC (K_i, 7.3 nM). TNP-UTP was identified as the most potent inhibitor for ACI (K_i, 7.1 nM) and ACII (K_i, 24 nM). TNP-NTPs inhibited sAC and GTP hydrolysis by G_s- and G_i-proteins only with low potencies. Molecular modeling revealed that TNP-GTP and TNP-ATP interact very similarly, but not identically, with VC1:IIC2. Collectively, our data show that TNP-nucleotides are useful fluorescent probes to monitor conformational changes in VC1:IIC2 and that TNP-NTPs are a promising starting point to develop isoform-selective AC and sGC inhibitors. TNP-ATP is the most potent sGC inhibitor known so far.

ACs catalyze the conversion of ATP into the second messenger cAMP and play a key role in signal transduction. In mammals, nine membranous AC isoforms (ACI–IX) have been identified (Defer et al., 2000; Sunahara and Taussig, 2002). mACs differ from each other in regulation and tissue expression, and studies with transgenic and gene-knock-out mice have revealed different functions for the various AC isoforms. Most strikingly, ACV is an important AC isoform in the heart (Göttle et al., 2009), and the knock-out of ACV protects mice against heart failure and induces longevity (Yan et al., 2007). Thus, ACV inhibitors may be valuable drugs for the treatment of cardiovascular diseases and ageing (Iwatsubo et al., 2004; Göttle et al., 2009). In addition to mACs, mammals express a structurally distinct sAC that is predominantly found in testis and is important for sperm maturation (Chen et al., 2000). Thus, sAC inhibitors may be promising candidates for male contraceptives (Schlicker et al., 2008). Finally, sGC, catalyzing the conversion of GTP into

This work was supported in part by the Deutsche Forschungsgemeinschaft [Grants Se529/5-1] (to R.S.); a predoctoral fellowship of the Studienstiftung des Deutschen Volkes (to A.G.); a predoctoral fellowship from the Elite Graduate Student Program of the Free State of Bavaria (to M.H.); and the National Institutes of Health [Grant R01-DK46371] (to S.R.S.).

[1] Current affiliation: Department of Microbiology and Molecular Genetics, Medical College of Wisconsin, Milwaukee, Wisconsin.

[2] Current affiliation: Research and Development, Cardiovascular Diseases, Sanofi-Aventis, Frankfurt/Main, Germany.

Article, publication date, and citation information can be found at http://jpet.aspetjournals.org.

doi:10.1124/jpet.109.155432.

ABBREVIATIONS: AC, adenylyl cyclase; mAC, membranous adenylyl cyclase; sAC, soluble adenylyl cyclase; β_2AR, β_2-adrenoceptor; $G_{i\alpha}$, inhibitory G-protein α-subunit; $G_{s\alpha S}$, short splice variant of the stimulatory G-protein α-subunit; $G_{s\alpha L}$, long splice variant of the stimulatory G-protein α-subunit; $G_{\alpha olf}$, olfactory G-protein α-subunit; sGC, soluble guanylyl cyclase; FPR, formyl peptide receptor; FS, forskolin; GPCR, G-protein-coupled receptor; DMB-FS, 7-acetyl-7-[*O*-(*N*-methylpiperazino)-γ-butyryl]-forskolin; MANT, 2′(3′)-*O*-(*N*-methylanthraniloyl); TNP, 2′,3′-*O*-(2,4,6-trinitrophenyl); VC1 and IIC2, the N- and C-terminal catalytic domains from canine type V mAC and rat type II mAC, respectively, expressed as soluble proteins; GTPγS, guanosine 5′-[γ-thio]triphosphate.

the second messenger cGMP, is a nucleotidyl cyclase structurally related to mAC (Sunahara et al., 1998). sGC is activated by NO, and NO-containing drugs are effective in the treatment of coronary heart disease and hypertensive crisis (Koesling et al., 2004; Derbyshire and Marletta, 2009; Schmidt et al., 2009). sGC inhibitors may be valuable experimental tools to study the role of this enzyme in cardiovascular and neuronal functions (Gille et al., 2004).

mACs are activated by the G-protein $G_{s\alpha}$ and require two divalent metal cations for catalysis (Sunahara and Taussig, 2002). ACs I–VIII are also activated by FS (Pinto et al., 2008, 2009). mACs consist of two membrane domains with six transmembrane helices each and two cytosolic domains. The two cytosolic domains, referred to as C1 and C2, form the catalytic core of AC, including the ATP-binding site, the FS-binding site, and the $G_{s\alpha}$-binding site, whereas the function of the transmembrane domains is as yet poorly defined (Sunahara and Taussig, 2002). Several crystal structures of the cytosolic domains of C1 and C2 (VC1:IIC2) in complex with $G_{s\alpha}$, FS, or DMB-FS and various nucleotides have been resolved, providing detailed insight into the mechanisms of catalysis and enzyme inhibition (Tesmer et al., 1997, 2000; Mou et al., 2005, 2006).

MANT-nucleotides (Hiratsuka, 1983; Jameson and Eccleston, 1997) are potent ACV inhibitors and block activation of voltage-dependent calcium channels in cardiomyocytes, but so far, the selectivity of mAC inhibitors is not satisfying (Gille et al., 2004; Rottlaender et al., 2007; Göttle et al., 2009). The MANT-group inserts like a wedge into a hydrophobic pocket between C1 and C2 and prevents transition of AC from the catalytically inactive closed to the catalytically active open conformation (Mou et al., 2005, 2006). Hydrophobic interactions between the MANT-group and C1:C2 pocket contribute very substantially to binding affinity, rendering MANT-nucleotides the most potent mAC inhibitors known so far (Gille et al., 2004; Mou et al., 2005; Göttle et al., 2009). Because the MANT-group is fluorescent and sensitive to changes in hydrophobicity (Hiratsuka, 1983; Jameson and Eccleston, 1997), the interaction of MANT-nucleotides with the hydrophobic pocket provided a unique opportunity to monitor nucleotide binding to and conformational changes of VC1:IIC2 (Mou et al., 2005, 2006; Pinto et al., 2009).

Because MANT-nucleotides are potent AC inhibitors but not particularly mAC isoform-specific, we went on to explore the interaction of other nucleotides with AC. Specifically, in a recent study, we showed that TNP-nucleotides (Hiratsuka, 2003) are also potent mAC inhibitors; i.e., TNP-ATP and TNP-GTP inhibit VCI:IIC2 in complex with $G_{s\alpha}$ and FS with K_i values in the 10 nM range (Mou et al., 2006). Crystallographic studies showed that the TNP-group binds to the same hydrophobic pocket as the MANT-group. Like MANT-nucleotides, TNP-nucleotides are fluorescent and sensitive to changes in hydrophobicity (Hiratsuka, 2003). Using the bacterial AC toxin from *Bordetella pertussis*, CyaA, as model system, we showed that MANT-nucleotides and TNP-nucleotides complement each other in the exploration of activation-dependent conformational changes in ACs (Göttle et al., 2007).

Therefore, the aims of the present study were to examine the interactions of VC1:IIC2 with TNP-nucleotides using fluorescence spectroscopy and to characterize the interactions of various ACs and sGC with TNP-nucleotides. Moreover, we examined the interaction of TNP-nucleotides with G-proteins obtain some information on selectivity of TNP-nucleotides for other relevant nucleotide-binding proteins involved in signal transduction. Previous studies from our laboratory showed that MANT-nucleotides bind to G-proteins with considerably lower affinity than to ACs (Gille and Seifert, 2003a,b).

Materials and Methods

Materials. VC1, IIC2, and VIIC were purified as described previously (Tesmer et al., 2002). The expression construct for glutathione *S*-transferase (GST)-human sAC was generated by cloning the coding region of human sAC (amino acid residues 1–470) into a pGEX-KG vector, in which a TEV protease recognition site was introduced before the start of the human sAC sequence. The plasmid was transformed into the expression strain *Escherichia coli* BL-21(DE3)-pLys and grown in Luria-Bertani medium containing ampicillin (50 μg/ml) until OD = 0.5. Thereafter, protein expression was induced with 30 μM isopropyl β-D-thiogalactopyranoside at 25°C for an additional 15 to 18 h. The harvested cells were suspended and sonicated in lysis buffer (50 mM Tris/HCl, pH 8.0, 50 mM NaCl, 5 mM dithiothreitol, and protease inhibitors). The crude cell lysate was centrifuged at 18,000*g* for 1 h at 4°C, and the supernatant fluid was loaded onto a 5-ml glutathione-Sepharose 4B resin column (GE Healthcare, Waukesha, WI). The GST-sAC protein was eluted from the resin with the aforementioned buffer containing 10 mM reduced glutathione (Sigma-Aldrich, St. Louis, MO). The pooled eluted fractions were digested overnight with TEV protease at 4°C. The TEV-digested protein was passed through a column with 1 ml of glutathione-Sepharose 4B resin and 0.5 ml of Talon resin (Clontech, Mountain View, CA) to remove the undigested protein, the GST tag, and TEV protease. Human sAC was dialyzed against a buffer consisting of 50 mM Tris/HCl, pH 7.5, 30 mM NaCl, 5 mM 2-mercaptoethanol, and protease inhibitors. The dialysate was applied onto a 30-ml Fast-Flow Q-Sepharose (GE Healthcare) and eluted with a 0 to 1 M NaCl gradient using an ÄKTA FPLC system (GE Healthcare). Purified human sAC protein was further passed through sizing columns to remove any remaining contaminants. The purity of the human sAC protein was >95% as determined by SDS polyacrylamide electrophoresis on a 4 to 20% (mass/vol) Tris-HCl polyacrylamide gel (Bio-Rad, Hercules, CA) and subsequent Coomassie Blue staining.

Baculoviruses encoding ACs I, II, and V were donated by Drs. A. G. Gilman and R. K. Sunahara (University of Texas Southwestern Medical Center, Dallas, TX). Purified sGC was from Alexis (Lausen, Switzerland). Construction and expression of β_2AR-$G_{s\alpha}$ and FPR-$G_{i\alpha}$ fusion proteins were described previously (Seifert et al., 1998; Wenzel-Seifert et al., 1999; Liu et al., 2001). Sf9 cells were obtained from the American Type Cell Culture Collection (Manassas, VA). TNP-ATP, TNP-ADP, and TNP-AMP were purchased from Invitrogen (Karlsruhe, Germany). TNP-GTP, TNP-GDP, TNP-UTP, and TNP-CTP were obtained from Jena Bioscience (Jena, Germany). DMB-FS was obtained from Calbiochem (La Jolla, CA). FS, 2′,5′-dideoxy-3′-ATP, myokinase, mono(cyclohexyl)ammonium phosphoenol pyruvate, and pyruvate kinase were obtained from Sigma-Aldrich. [α-^{32}P]ATP (3000 Ci/mmol), [α-^{32}P]GTP (3000 Ci/mmol), and [γ-^{32}P]GTP (6000 Ci/mmol) were purchased from PerkinElmer Life and Analytical Sciences (Boston, MA). Sources of cell culture reagents and other materials have been described previously (Wenzel-Seifert et al., 1999; Gille and Seifert, 2003a; Gille et al., 2004; Mou et al., 2006).

Cell Culture and Membrane Preparation. Cell culture, expression, and membrane preparation were carried out as described previously (Wenzel-Seifert et al., 1999; Gille et al., 2004). In brief, Sf9 cells were cultured in SF 900 II medium (Invitrogen) with 5% (v/v) fetal bovine serum and 0.1 mg/ml gentamycin. Sf9 cells were infected with 1:100 dilutions of baculoviruses encoding different ACs

or GPCR-G_α fusion proteins and cultured for 48 h. Cells were then harvested by centrifugation for 10 min (1000*g* at 4°C). Pellets were resuspended in lysis buffer (10 mM Tris/HCl, 1 mM EDTA, 0.2 mM phenylmethylsulfonyl fluoride, 10 μg/ml leupeptin, and 10 μg/ml benzamide, pH 7.4) and disrupted with 20 strokes using a Dounce homogenizer. The resultant suspension was centrifuged for 5 min (500*g* at 4°C) for sedimentation of nuclei. The supernatant fluid containing the cell membranes was transferred to 30-ml tubes and centrifuged for 20 min (30,000*g* at 4°C). The resultant pellet was then collected and resuspended in storage buffer containing 75 mM Tris/HCl, 12.5 mM $MgCl_2$, and 1 mM EDTA, pH 7.4. Protein concentration for each membrane was measured using a Bio-Rad DC protein assay kit. Membrane aliquots (0.5–1 ml each) were stored at −80°C.

AC and GC Activity Assay. The AC activity assay with VC1:IIC2 was performed as described previously (Mou et al., 2005, 2006). Assay tubes contained 7 nM VCI and 35 nM IIC2. TNP-nucleotides (final concentration, 1 nM-100 μM) were added. After a preincubation for 2 min at 30°C, 20 μl of reaction mixture containing (final) 100 μM cAMP, 40 μM ATP, 10 mM $MnCl_2$, 100 mM KCl, 25 mM HEPES/NaOH, pH 7.4, and 1.0–1.5 μCi/tube [α-^{32}P]ATP were added to assay tubes. After incubation for 1 h at 30°C, reactions were terminated by adding 20 μl of 2.2 N HCl. Denatured protein was sedimented by a 1-min centrifugation at 25°C and 15,000*g* followed by application of 65 μl of the supernatant fluid onto disposable alumina columns containing 1.3-g neutral alumina (Sigma A-1522, super I, WN-6; Sigma-Aldrich). To separate [^{32}P]cAMP from [^{32}P]ATP, 4 ml of 0.1 M ammonium acetate was added for elution of [^{32}P]cAMP. Recovery of [^{32}P]cAMP was approximately 80% as assessed with [^{3}H]cAMP set as standard. [^{32}P]cAMP was determined by liquid scintillation counting using Ecolume scintillation cocktail. AC assays with membranes from Sf9 cells expressing ACs I, II, and V were conducted as described previously (Gille et al., 2004). Membranes were first centrifuged for 15 min (15,000*g* at 4°C), and the pellets were resuspended in storage buffer. Each assay tube contained membranes expressing an AC isoform (15–20 μg of protein/tube), 10 μM GTPγS, 40 μM ATP, 100 μM FS, 1 mM $MnCl_2$ and 100 μM cAMP. Reactions were conducted for 20 min at 30°C. Reaction mixtures for sAC contained 200 ng of purified sAC, 50 mM Tris/HCl, pH 7.4, 5 mM $MnCl_2$, 10 mM $CaCl_2$, 40 μM ATP, 1.0–1.5 μCi/tube [α-^{32}P]ATP, and 100 μM cAMP. In some experiments, we assessed the effect of an NTP-regenerating system consisting of 2.7 mM mono(cyclohexyl)ammonium phosphoenol pyruvate, 0.125 IU pyruvate kinase, and 1 IU myokinase on the inhibitory potency of TNP-AMP and TNP-ADP.

sGC activity was determined as described previously (Gille et al., 2004). In brief, reaction mixtures contained 0.2% (mass/vol) bovine serum albumin, 5 ng of purified sGC, 30 mM Tris/HCl, pH 7.4, 5 mM $MnCl_2$, 20 μM GTP, 1.0–1.5 μCi [α-^{32}P]GTP, 100 μM cGMP, 100 μM sodium nitroprusside, and TNP-nucleotides (final concentration, 1 nM-100 μM). [^{32}P]cGMP was separated from [α-^{32}P]GTP as described for the [^{32}P]cAMP/[α-^{32}P]ATP pair.

Fluorescence Spectroscopy. All experiments were carried out using a Cary Eclipse fluorescence spectrophotometer at 25°C (Varian Inc., Walnut Creek, CA) as described previously (Mou et al., 2005, 2006; Göttle et al., 2007; Pinto et al., 2009). In brief, measurements were performed using a quartz fluorescence microcuvette (Hellma, Plainview, NY) in a final assay volume of 150 μl. Steady-state emission spectra were recorded at low speed with λ_{ex} = 405 nm (λ_{em} = 500–600 nm). Reaction mixtures contained 100 mM KCl and 10 mM $MnCl_2$ in 25 mM HEPES/NaOH, pH 7.4, followed by sequential addition of TNP-nucleotides (final concentration, 5 μM), 4 μM VCI plus 25 μM IIC2, and 100 μM final DMB-FS (water-soluble analog of FS).

In contrast to MANT-nucleotides, in TNP-nucleotides, the fluorescent TNP-group does not isomerize between the 2′- and 3′-*O*-ribosyl position since the TNP substituent is linked to both the 2′- and 3′-*O*-ribosyl position simultaneously. Accordingly, TNP-nucleotides are more rigid molecules than MANT-nucleotides (Hiratsuka, 1983, 2003; Jameson and Eccleston, 1997). Another difference between MANT-nucleotides and TNP-nucleotides is the fact that the latter nucleotides exhibit a much lower basal fluorescence than the former nucleotides, increasing the potential signal-to-noise ratio in fluorescence studies (Göttle et al., 2007). Moreover, TNP-nucleotides are excited in the visible light range (λ_{ex}, 405 nm), whereas MANT-nucleotides are excited in the UV light range (λ_{ex}, 350 nm). Thus, fluorescence studies with TNP-nucleotides are less sensitive to interference with substances absorbing UV light. In MANT-nucleotides, the fluorescent MANT-group can spontaneously isomerize between the 2′- and 3′-*O*-ribosyl position at physiological pH (Hiratsuka, 1983; Jameson and Eccleston, 1997). Accordingly, MANT-nucleotides are not clearly defined at any given time.

GTPase Assay. Steady-state GTPase activity was determined as described previously (Seifert et al., 1998; Wenzel-Seifert et al., 1999; Liu et al., 2001). In brief, membranes from Sf9 cells expressing β_2AR-$G_{s\alpha}$ and FPR-$G_{i\alpha}$ fusion proteins were thawed and centrifuged for 15 min (15,000*g* at 4°C) to eliminate any endogenous nucleotides. Pellets were resuspended in 10 mM Tris/HCl, pH 7.4. Assay tubes contained 10 μg of protein/tube, 1 mM adenylyl imidodiphosphate, 100 nM unlabeled GTP, 100 μM ATP, 1 mM $MgCl_2$, 100 μM EDTA, 0.2% (mass/vol) bovine serum albumin, 5 mM creatine phosphate, and 40 μg of creatine kinase in 50 mM Tris/HCl, pH 7.4, and increasing concentrations of TNP-ATP or TNP-GTP ranging from 1 μM to 1 mM and 10 μM isoproterenol (agonist for β_2AR-$G_{s\alpha}$) or 10 μM *N*-formyl-L-methionyl-L-leucyl-L-phenylalanine (agonist for FPR-$G_{i\alpha}$) to fully activate GPCRs and, consequently, GTP hydrolysis by G-proteins. Assay tubes with the reaction mixtures were incubated for 3 min at 25°C following addition of 20 μl of [γ-^{32}P]GTP (0.2 μCi/tube). Reactions were carried out for 20 min at 25°C and terminated by adding 900 μl of slurry (5% mass/vol activated charcoal and 50 mM NaH_2PO_4, pH 2.0). Reaction mixtures were centrifuged for 15 min (15,000*g* at room temperature). Seven hundred microliters of supernatant fluid were removed from assay tubes, and $^{32}P_i$ was determined by liquid scintillation counting. In the presence of 1 mM unlabeled GTP, nonenzymatic degradation of [γ-^{32}P]GTP was determined and was <1% of the total amount of radioactivity added.

Molecular Modeling. Docking calculations were carried out using the GOLD 3.0.1 docking software. As starting point, we used the crystal structure of VC1:IIC2:FS:$G_{s\alpha\text{-}GTP\gamma S}$ in complex with TNP-ATP and two Mn^{2+} ions (Protein Data Bank ID: 1GVD) (Mou et al., 2006). The bound ligand, TNP-ATP, was used as reference for determination of the binding of TNP-GTP. All atoms and their associated residues within 5 Å of each ligand atom were used to define the catalytic site. The information on ligand hydrogen-bonding interactions and conformations was encoded into the corresponding genetic algorithm (GA) of GOLD, using the default GOLD 3.0.1 GA parameter. The Goldscore and Chemscore scoring functions were used to rank binding poses. Exogenous TNP-ATP was aligned to the bound TNP-ATP conformation in the VC1:IIC2 crystal structure. The docked conformation of the optimally aligned TNP-ATP model mimicked the interactions observed in the crystal structure. Thus, the rigid docking procedure reproduced actual ligand/enzyme interactions. The molecular surface of VC1:IIC2 was calculated with the PYMOL software.

Data Analysis. All inhibition curves were analyzed by nonlinear regression using Prism 4.0 software (GraphPad, San Diego, CA). Fluorescence spectra were analyzed using the spectrum package of the Cary Eclipse software. For generation of graphs shown in Figs. 1 and 2, data were imported into the Prism software.

Results

Inhibition of the Catalytic Activity of VC1:IIC2 by TNP-Nucleotides. VC1:IIC2 possesses a broad specificity for purine and pyrimidine nucleotides as is reflected by the fact that the fully activated enzyme, i.e., VC1:IIC2 in the

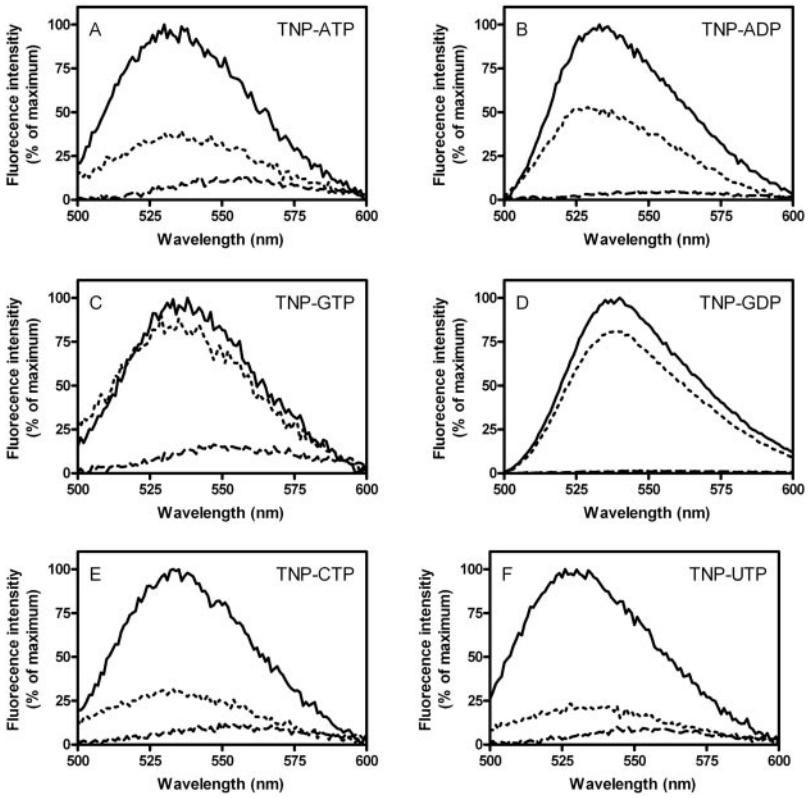

Fig. 1. Fluorescence emission spectra of TNP-nucleotides in the absence and presence of VC1:IIC2 and DMB-FS. Fluorescence experiments were performed as described under *Materials and Methods*. Steady-state emission spectra of TNP-nucleotides were recorded at λ_{ex} = 405 nm and λ_{em} = 500 to 600 nm. Cuvettes contained TNP-nucleotides (5 μM each) in the absence or presence of VC1:IIC2 and 100 μM DMB-FS. Fluorescence intensities are expressed as percentage of the maximal emission in the respective experiment and were analyzed using the spectrum package of the Cary Eclipse software. A, TNP-ATP. B, TNP-ADP. C, TNP-GTP. D, TNP-GDP. E, TNP-CTP. F, TNP-UTP. Dashed lines represent emission spectra for TNP-nucleotides alone; solid lines represent spectra in the presence of TNP-nucleotides plus VC1:IIC2; and dotted lines represent spectra in the presence of TNP-nucleotides plus VC1:IIC2 plus DMB-FS. Representative fluorescence tracings are shown. Similar results were obtained in three to four independent experiments.

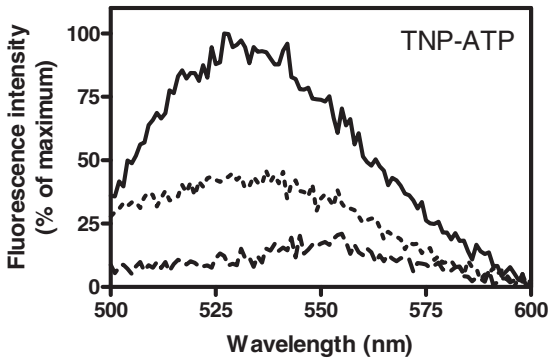

Fig. 2. Fluorescence emission spectra of TNP-ATP in the absence and presence of VC1:IIC2 and 2′,5′-dideoxy-3′-ATP. Fluorescence experiments were performed as described under *Materials and Methods*. Steady-state emission spectra of TNP-ATP were recorded at λ_{ex} = 405 nm and λ_{em} = 500 to 600 nm. Cuvettes contained TNP-ATP (5 μM) in the absence or presence of VC1:IIC2 and 200 μM 2′,5′-dideoxy-3′-ATP. Fluorescence intensities are expressed as percentage of the maximal emission and were analyzed using the spectrum package of the Cary Eclipse software. The dashed line represents the emission spectrum of TNP-ATP alone; the solid line represents the spectrum in the presence of VC1:IIC2; and the dotted line represents the spectrum in the presence of VC1:IIC2 plus 2′,5′-dideoxy-3′-ATP. Representative fluorescence tracings are shown. Similar results were obtained in three independent experiments.

presence of FS and $G_{s\alpha\text{-}GTP\gamma S}$, was inhibited with similar potency by TNP-ATP, TNP-GTP, and TNP-UTP, followed by TNP-CTP (Mou et al., 2006). In the presence of FS alone, TNP-ATP, TNP-UTP, and TNP-CTP were about equally potent VC1:IIC2 inhibitors, followed by TNP-GTP. The omission of $G_{s\alpha\text{-}GTP\gamma S}$ had only minor effects on overall TNP-nucleotide potency (Mou et al., 2006).

For fluorescence studies with TNP-nucleotides, it was important to determine whether TNP-nucleotides can also bind to VC1:IIC2 in the absence of activators (Mou et al., 2005, 2006). In fact, in the absence of the activators FS and $G_{s\alpha\text{-}GTP\gamma S}$, TNP-NDPs and TNP-NTPs inhibited the catalytic activity of VC1:IIC2, with potencies that differed from each other by <5-fold (Table 1). However, compared to the conditions with FS, the potencies of TNP-NTPs were reduced by up to 150-fold in the absence of FS (Mou et al., 2006).

Fluorescence Studies with VC1:IIC2 and TNP-Nucleotides. In agreement with previous data (Hiratsuka, 2003; Göttle et al., 2007), TNP-nucleotides exhibited only small fluorescence signals in the absence of VC1:IIC2 (Fig. 1). However, VC1:IIC2 largely increased these fluorescence signals with TNP-ATP, TNP-ADP, TNP-GTP, TNP-GDP, TNP-CTP, and TNP-UTP, compatible with the assumption that TNP-nucleotides bind to the enzyme and that the TNP-group inserts into the hydrophobic pocket between VC1 and IIC2 that is also occupied by MANT-nucleotides (Mou et al., 2005, 2006). In the absence of VC1:IIC2, TNP-nucleotides exhibited an emission maximum of 545 nm (Table 2). The addition of VC1:IIC2 shifted the emission maximum toward shorter wavelengths, a process referred to as blue-shift. The blue-shift exhibited nucleotide-specific differences, with TNP-GDP showing the smallest shift and TNP-UTP showing the largest shift.

The nonfluorescent ATP analog, 2′,5′-dideoxy-3′-ATP, binds to the catalytic site of VC1:IIC2 with high affinity (Tesmer et al., 2000; Gille et al., 2004). To assess the specificity of the fluorescence increases of TNP-nucleotides upon addition of VC1:IIC2, we examined the effect of 2′,5′-dideoxy-3′-ATP. In fact, 2′,5′-dideoxy-3′-ATP (200 μM) strongly reduced the fluorescence increase of TNP-ATP (5 μM) caused by the addition of VC1:IIC2 (Fig. 2). These data show that

TABLE 1

Inhibition of VC1:IIC2 by TNP-nucleotides

AC activity was determined as described under *Materials and Methods* in the presence of Mn^{2+}. Reaction mixtures contained TNP-nucleotides at concentrations from 1 nM to 100 μM as appropriate to generate saturated inhibition curves. Inhibition curves were analyzed by nonlinear regression and were best-fitted to monophasic sigmoidal curves. K_i values were calculated from IC_{50} values using the previously determined K_m values (Mou et al., 2005). Data shown are the means ± S.D. of three to six experiments performed in duplicates.

TNP-Nucleotide	K_i
	nM
TNP-AMP	> 100,000
TNP-ADP	11,000 ± 5900
TNP-ATP	3300 ± 1400
TNP-GDP	15,000 ± 1000
TNP-GTP	6400 ± 2000
TNP-UTP	14,000 ± 1200
TNP-CTP	8600 ± 1100

TNP-nucleotides and 2′,5′-dideoxy-3′-ATP compete for binding to the catalytic site of VC1:IIC2.

The addition of the water-soluble FS-analog, DMB-FS (Pinto et al., 2008, 2009), to cuvettes containing TNP-nucleotides and VC1:IIC2 decreased the fluorescence signals of TNP-nucleotides (Fig. 1). However, TNP-nucleotides exhibited large differences in their sensitivity toward reduction of fluorescence upon addition of DMB-FS. Specifically, with TNP-ATP, TNP-CTP, and TNP-UTP, large decreases in fluorescence were observed, whereas the decrease was moderate with TNP-ADP and only marginal with TNP-GTP and TNP-GDP.

Molecular Modeling of the Interaction of TNP-GTP and TNP-ATP with VC1:IIC2. To obtain direct evidence for distinct interactions of TNP-nucleotides with VC1:IIC2, we undertook substantial efforts to produce a crystal structure of VC1:IIC2 in complex with $G_{s\alpha\text{-}GTP\gamma S}$, Mn^{2+} and TNP-GTP. Unfortunately, our efforts have been unsuccessful for unknown reasons (data not shown). Therefore, as an alternative approach, we conducted molecular modeling studies. Using the crystal structure of VC1:IIC2 in complex with TNP-ATP as template (Mou et al., 2006), TNP-GTP was docked into the catalytic site of the enzyme (Fig. 3). Overall, TNP-ATP and TNP-GTP adopt similar positions in the catalytic site, and both nucleotides interact with the amino acids Asn1025 and Lys1065 of IIC2 (Fig. 3A) (Mou et al., 2006). Figure 3A also shows the insertion of the TNP-group into the hydrophobic pocket between IIC2 and VC1, providing an explanation for the fluorescence increase of TNP-nucleotides upon binding to the enzyme (Fig. 1). Although TNP-ATP and TNP-GTP bind to VC1:IIC2 similarly, there are also subtle differences. In particular, the N2-atom of guanine forms a hydrogen bond with Asp1018, resulting in slightly different orientations of both the triphosphate chain and the TNP-group (Fig. 3B).

Inhibition of the Catalytic Activity of AC Isoforms and sGC by TNP-Nucleotides. ACV inhibitors may be valuable drugs for the treatment of cardiovascular diseases, specifically chronic heart failure (Iwatsubo et al., 2004; Rottlaender et al., 2007; Yan et al., 2007; Göttle et al., 2009), and sAC inhibitors may represent a novel class of male contraceptives (Schlicker et al., 2008). Therefore, we systematically studied the potencies of TNP-nucleotides for inhibition of ACs I, II, and V and sAC (Table 3). We also included sGC into our studies because this enzyme is structurally related to membranous ACs (Sunahara et al., 1998) and exhibits broad-base specificity as well (Gille et al., 2004). Moreover, sGC plays an important role in the regulation of numerous cardiovascular and neuronal processes, but there is a paucity of potent and selective substrate-binding site-based sGC inhibitors (Derbyshire and Marletta, 2009; Schmidt et al., 2009).

TNP-nucleotides inhibited ACI in the order of potency TNP-UTP ~ TNP-ATP > TNP-GTP ~ TNP-CTP > TNP-ADP > TNP-GDP ⋙ TNP-AMP (Table 3). ACII was less sensitive to inhibition by TNP-nucleotides than ACI. These data are in agreement with the results obtained with MANT-nucleotides (Gille et al., 2004; Göttle et al., 2009). However, we also noted that the order of potency of TNP-nucleotides for inhibition of ACs I and II was different. Specifically, the order of potency for ACII was TNP-UTP > TNP-ATP ~ TNP-CTP > TNP-GTP ≫ TNP-ADP > TNP-GDP > TNP-AMP (Table 3). Like ACI, ACV showed high sensitivity to inhibition by TNP-nucleotides. These data are again in agreement with the results obtained with MANT-nucleotides (Gille et al., 2004; Göttle et al., 2009). However, the inhibitor profiles were different for both AC isoforms. Specifically, TNP-nucleotides inhibited ACV in the order of potency: TNP-ATP > TNP-UTP > TNP-GTP ~ TNP-CTP ≫ TNP-ADP > TNP-GDP > TNP-AMP (Table 3). The substantial loss of potency of TNP-ADP and TNP-AMP relative to TNP-ATP, as well as TNP-GDP relative to TNP-GTP, in all mACs studied is explained by the loss of ionic interactions between the β- and γ-phosphates with Lys1065 of IIC2 and metal ion B (Mou et al., 2006).

In accordance with the data obtained for MANT-nucleotides (Gille et al., 2004), sAC was considerably less sensitive to inhibition by TNP-nucleotides than mACs. Among the compounds examined, TNP-ATP was the most potent sAC inhibitor, but the nucleotide was 7- to 200-fold less potent than at ACs I, II, and V (Table 3). These data show that the structure/activity relationships for nucleotide-based inhibitors of mACs and sAC are quite different and that it will be very challenging to obtain highly potent AC inhibitors with selectivity relative to mACs.

In marked contrast, sGC was very sensitive to inhibition by TNP-nucleotides, with ACV and sGC showing substantial similarities in the inhibition profile (Table 3). TNP-ATP was a slightly more potent sGC inhibitor than TNP-GTP. Notably, the pyrimidine nucleotides TNP-UTP and TNP-CTP were just 3- to 5-fold less potent sGC inhibitors than the

TABLE 2

Emission peaks of TNP-nucleotides in the absence and presence of VC1:IIC2

Fluorescence experiments were performed as described under *Materials and Methods*. Steady-state emission spectra of TNP-nucleotides in the presence of Mn^{2+} were recorded at λ_{ex} = 405 nm and λ_{em} = 500 to 600 nm in the absence or presence of VC1:IIC2. The concentration of TNP-nucleotides was 5 μM each. The blue-shift is the difference between the emission maximum in the absence and presence of VC1:IIC2. Fluorescence recordings were calculated with the spectrum package of the Cary Eclipse software. Data shown are the means ± S.D. of three to four independent experiments.

TNP-Nucleotide	Emission Peak in the Absence of VC1:IIC2	Emission Peak in the Presence of VC1:IIC2	Blue-Shift of Emission Peak
		nm	
TNP-ADP	545 ± 1	532 ± 1	13 ± 1
TNP-ATP	545 ± 2	532 ± 2	14 ± 2
TNP-GDP	545 ± 1	540 ± 1	5 ± 1
TNP-GTP	545 ± 1	537 ± 1	8 ± 1
TNP-UTP	545 ± 3	528 ± 3	17 ± 3
TNP-CTP	545 ± 1	532 ± 1	13 ± 1

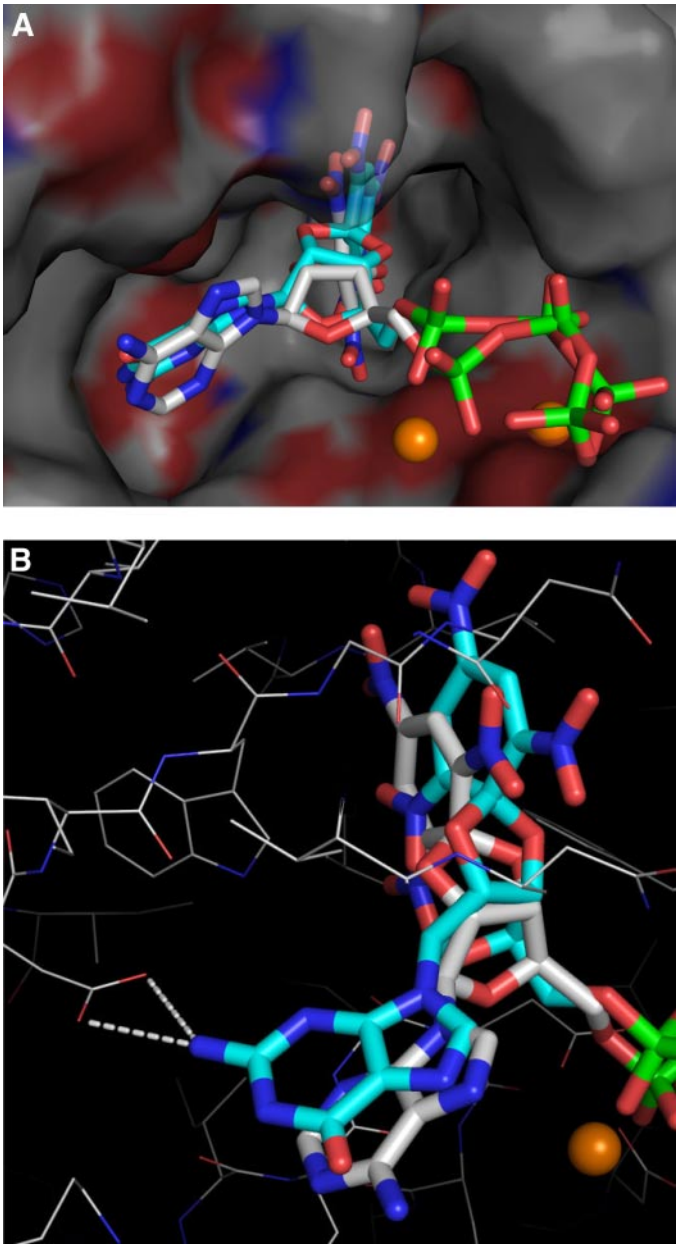

Fig. 3. Model of TNP-ATP and TNP-GTP binding to VC1:IIC2. Docking studies were performed as described under *Materials and Methods*. The crystal structure of VC1:IIC2:FS:$G_{s\alpha\text{-}GTP\gamma S}$:TNP-ATP (Protein Data Bank ID: 1GVD) served as template for docking TNP-GTP into the catalytic site. Docking calculations were carried out using the GOLD 3.0.1 software. A, superimposition of TNP-ATP and TNP-GTP in the catalytic core of VC1:IIC2. Ligands are shown as stick models; carbon atoms are gray for TNP-ATP and cyan for TNP-GTP. Nitrogen, oxygen, and phosphorus atoms are shown in blue, red, and green, respectively. Mn^{2+} is shown as orange sphere. The AC surface is shown as a solvent-accessible molecular surface: red representing acidic surfaces, blue representing basic surfaces, and gray representing hydrophobic surfaces. B, detailed view of the superimposition of TNP-ATP and TNP-GTP in the catalytic core of VC1:IIC2, with the molecular surface removed. In the bottom left corner, the hydrogen bonds between N2 of the guanine ring and Asp1018 are shown.

purine nucleotides. To the best of our knowledge, TNP-ATP is the most potent sGC inhibitor reported so far (Derbyshire and Marletta, 2009; Schmidt et al., 2009). Cell membrane-permeable TNP-nucleotides may become very valuable tools for the analysis of sGC in cardiovascular and neuronal functions. Moreover, TNP-nucleotides may be useful ligands for crystallizing sGC, of which the goal has not yet been accomplished.

Inhibition of the Catalytic Activity of G_s- and G_i-Proteins by TNP-Nucleotides. The steady-state GTPase assay with GPCR-G_α fusion proteins is a very well suited assay for the determination of G_i- and G_s-protein affinities for nucleotides (Seifert et al., 1999; Gille et al., 2002, 2005; Gille and Seifert, 2003b). In a previous study we showed that MANT-guanosine 5′-[γ-thio]triphosphate and MANT-guanosine 5′-[β,γ-imido]triphosphate bind to G_i- and G_s-proteins with low-affinity, i.e., in the 0.2 to 1.0 μM and 1 to 6 μM range, respectively (Gille and Seifert, 2003b). This low-affinity interaction of MANT-nucleotides is explained by the tight guanine nucleotide-binding pocket of G-protein α-subunits, leaving little space to accommodate bulky substituents at the 2′- and 3′-*O*-ribosyl position (Seifert and Gille, 2003b). Accordingly, we expected the conformationally constrained TNP-nucleotides also to bind to G-proteins with low affinity. Indeed, TNP-GTP inhibited the agonist-stimulated steady-state GTP hydrolysis of various β_2AR-$G_{s\alpha}$ and FPR-$G_{i\alpha}$ fusion proteins only with K_i values in the 10 to 30 μM range (Table 4). Considering then that TNP-GTP inhibits holo-ACs and sGC with K_i values in the 10 to 200 nM range (Table 3), it becomes clear that TNP-GTP exhibits an exquisite selectivity for nucleotidyl cyclases compared with G-proteins. TNP-ATP binds to G_s- and G_i-proteins with even lower affinity than TNP-GTP, i.e., with K_i values >50 to 100 μM. Thus, TNP-ATP exhibits >1000-fold selectivity for some ACs relative to G-proteins. The low affinity of G-proteins for TNP-GTP also implies that this nucleotide is very unlikely to be useful as fluorescent probe for monitoring conformational changes in G-proteins.

Discussion

TNP-Nucleotides as Experimental Tools. TNP-nucleotides are broadly used as fluorescence probes for many nucleotide-binding proteins, including receptors, enzymes, and structural proteins (Hiratsuka, 2003). To the best of our knowledge, mACs exhibit the highest affinity for TNP-nucleotides among all target proteins studied so far (Table 3). Most proteins bind TNP-nucleotides with affinities in the micromolar range (Hiratsuka, 2003), whereas several ACs and sGC exhibit affinities for TNP-nucleotides in the nanomolar range (Tables 1 and 3) (Mou et al., 2006). Moreover, TNP-nucleotides possess an excellent selectivity for mACs relative to G-proteins (Table 4). This striking selectivity of TNP-nucleotides for mACs relative to G-proteins could be exploited in electrophysiological signal transduction studies with intact cells in which nucleotides are introduced as AC inhibitors into the cytosol via the patch pipette (Rottlaender et al., 2007).

Broad-Base Specificity of ACs and sGC. Our present study corroborates the unexpected notion that mACs exhibit a broad-base specificity and high conformational flexibility (Gille and Seifert, 2003; Gille et al., 2004; Mou et al., 2005, 2006; Göttle et al., 2009). This notion can be extended to structurally unrelated bacterial AC toxins (Göttle et al., 2007; Taha et al., 2009) and, as shown here, to sGC and sAC (Table 3). Thus, despite the substantial structural differences between all of the nucleotidyl cyclases studied so far (Sunahara et al., 1998; Sunahara and Taussig, 2002; Ahuja et

TABLE 3

Inhibition of various AC isoforms and sGC by TNP-nucleotides

mAC, sAC, and sGC activity was determined as described under *Materials and Methods* in the presence of Mn^{2+}. Reaction mixtures contained TNP-nucleotides at concentrations from 1 nM to 100 μM as appropriate to generate saturated inhibition curves. Inhibition curves were analyzed by nonlinear regression and were best-fitted to monophasic sigmoidal curves. K_i values were calculated from IC_{50} values using the previously determined K_m values (Gille et al., 2004). K_m for sAC was 380 ± 20 μM, and V_{max} was 760 nmol/mg/min. Data shown are the means ± S.D. of three to six experiments performed in duplicates.

TNP-Nucleotide	K_i ACI	K_i ACII	K_i ACV	K_i sAC	K_i sGC
			nM		
TNP-AMP	4800 ± 1000	7400 ± 520	4800 ± 1200	N.D.	N.D.
TNP-ADP	140 ± 17	1100 ± 180	370 ± 45	N.D.	N.D.
TNP-ATP	9.0 ± 4.1	99 ± 2.7	3.7 ± 1.0	710 ± 82	7.3 ± 1.7
TNP-GDP	410 ± 76	3400 ± 1300	1200 ± 280	N.D.	N.D.
TNP-GTP	23 ± 2.2	220 ± 30	27 ± 4.3	7200 ± 280	8.6 ± 2.6
TNP-UTP	7.1 ± 2.3	24 ± 8.4	15 ± 2.2	3100 ± 50	33 ± 6.9
TNP-CTP	24 ± 2.9	110 ± 35	31 ± 3.9	5100 ± 480	27 ± 0.9

N.D., not determined.

TABLE 4

Affinities of G_s- and G_i-proteins for TNP-ATP and TNP-GTP

High-affinity GTPase activity in Sf9 membranes expressing various GPCR-G_α fusion proteins was determined as described under *Materials and Methods* in the presence of Mg^{2+}. Reaction mixtures contained TNP-nucleotides at concentrations from 1 nM to 100 μM as appropriate to generate saturated inhibition curves. Inhibition curves were analyzed by nonlinear regression and were best-fitted to monophasic sigmoidal curves. K_i values were calculated from IC_{50} values using the previously determined K_m values (Gille and Seifert, 2003b). Data shown are the means ± S.D. of three experiments performed in duplicates.

Construct	K_i TNP-ATP	K_i TNP-GTP
	nM	
β_2AR-$G_{s\alpha S}$	53,000 ± 11,000	12,000 ± 1500
β_2AR-$G_{s\alpha L}$	>100,000	17,000 ± 2100
β_2AR-$G_{\alpha olf}$	>100,000	26,000 ± 3400
FPR-$G_{i\alpha 1}$	>100,000	12,000 ± 3100
FPR-$G_{i\alpha 2}$	>100,000	6900 ± 1300
FPR-$G_{i\alpha 3}$	>100,000	10,000 ± 2200

al., 2004), broad-base specificity is a common and highly conserved theme in this enzyme class. The broad-base specificity and conformational flexibility, however, do not imply that all nucleotidyl cyclases exhibit identical pharmacological profiles. In fact, each nucleotidyl cyclase exhibits a unique profile (Table 3). Moreover, the differential effects of DMB-FS and the differences in blue-shift in our fluorescence studies revealed that purine and pyrimidine nucleotides bind to the catalytic site of at least one AC (VCI:IIC2) in slightly different manners (Fig. 1; Table 2).

We also would have liked to have conducted fluorescence studies with sGC that based on the high affinity of this enzyme for TNP-nucleotides are technically feasible. However, a drawback of the fluorescence studies is the fact that high protein concentrations (in the 5–25 μM range) are required (see *Materials and Methods*). Unfortunately, it is not yet possible to obtain such large amounts of sGC. Conversely, large amounts of recombinant sAC can be readily obtained (see *Materials and Methods*), but the affinity of sAC for TNP-nucleotides is too low for fluorescence studies (Table 3).

Whereas MANT-nucleotides are more potent inhibitors of VC1:IIC2 than of holo-ACs I and V (Gille et al., 2004), the opposite is true of TNP-nucleotides (Tables 1 and 3) (Mou et al., 2006). Thus, the structural constraints in TNP-nucleotides caused by the dual and nonisomerizing 2′- and 3′-*O*-ribosyl modification compared with the isomerizing 2′- and 3′-*O*-ribosyl isomerization in MANT-nucleotides (Jameson and Eccleston, 1997; Hiratsuka, 2003) facilitate binding to holo-ACs. A major structural difference between VC1:IIC2 and holo-ACs is that the former enzyme is completely devoid of the transmembrane domains (Sunahara and Taussig, 2002). These data indicate that the transmembrane domains, perhaps by modulation of the mobility of the catalytic domains, differentially regulate inhibitor affinities of holo-ACs.

The high affinity of ACs I, II, and V and sGC for TNP-UTP and TNP-CTP is quite remarkable. These data raise the intriguing question whether UTP and CTP can also be substrates for ACs. In support of such a possibility is the fact that both 3′,5′-cyclic CMP and 3′,5′-cyclic UMP do, indeed, occur in mammalian tissues as shown by sensitive mass spectrometry techniques (Newton et al., 1984, 1986). Moreover, in experiments with [α-^{32}P]UTP as substrate, [^{32}P]cUMP was identified as a bona fide product of sGC (Gille et al., 2004), but direct structural confirmation of cUMP production by sGC with mass spectrometry techniques is still missing. The structural identity of the putative mammalian cytidylyl cyclase is elusive as well (Newton et al., 1990).

Comparison of TNP-Nucleotides and MANT-Nucleotides as Fluorescence Probes. The crystal structures of VC1:IIC2 with MANT-GTP, MANT-ATP, and TNP-ATP show that, in all three cases, the fluorescent group, be it a MANT-group or a TNP-group, resides in a hydrophobic pocket between the VC1 and IIC2 subunit (Mou et al., 2005, 2006). Because both MANT-nucleotides and TNP-nucleotides respond with an increase in fluorescence upon exposure to a hydrophobic environment (Jameson and Eccleston, 1997; Hiratsuka, 2003), one may have predicted to observe similar fluorescence changes with both classes of nucleotides upon interaction with VC1:IIC2. However, this was clearly not the case. Most strikingly, even in the absence of DMB-FS, VC1:IIC2 caused large fluorescence increases with TNP-nucleotides and blue-shifts of the emission maximum (Fig. 1; Table 2), indicating that the hydrophobic pocket between both subunits can already form in the absence of AC activators. In contrast, MANT-nucleotides are quite ineffective at inserting into the hydrophobic pocket of VCI:IIC2 in the absence of activators (Mou et al., 2005, 2006). Whereas FS translocates the MANT-group into a more hydrophobic environment, resulting in fluorescence increases (Mou et al., 2005, 2006; Pinto et al., 2009), FS translocates the TNP-group into a more hydrophilic environment, resulting in fluorescence decreases. Intriguingly, both among MANT-nucleotides (Mou et al., 2006) and TNP-nucleotides (Fig. 1; Table 2), there are substantial base-specific differences in fluorescence properties. Those differences were not predicted either by crystallographic studies (Mou et al., 2006) or molecular modeling studies (Fig. 3). Thus, fluorescence spectroscopy is much more sensitive than crystallography and molecular modeling

at revealing very subtle conformational differences among similar ligands bound to mAC. These data corroborate the concept of conformational flexibility of ACs.

There are also some interesting similarities in the fluorescence properties of MANT-nucleotides and TNP-nucleotides at VC1:IIC2 compared with the bacterial AC toxin CyaA that is activated by calmodulin. Specifically, with MANT-nucleotides, there is an increase in direct fluorescence and fluorescence resonance energy transfer upon interaction of CyaA with calmodulin, whereas with TNP-nucleotides, there is a calmodulin-dependent decrease in fluorescence (Göttle et al., 2007). The mAC activator FS revealed similar patterns with MANT- and TNP-nucleotides at VCI:IIC2 (Mou et al., 2005, 2006; Pinto et al., 2009) (Fig. 2). Moreover, the fluorescence decreases with TNP-nucleotides at CyaA are, like with VC1:IIC2, base-dependent. Strikingly, the activation-dependent decreases in fluorescence at CyaA and VC1:IIC2 with TNP-nucleotides were most prominent for the pyrimidine bases (Göttle et al., 2007). These data indicate that, despite the substantial structural differences between mammalian membranous ACs and the bacterial AC toxin (Sunahara and Taussig, 2002; Ahuja et al., 2004), there are common and highly conserved themes in activation-dependent conformational changes in both classes of enzymes. Probably, these conserved conformational changes are directly related to the broad-base specificity found in mACs and bacterial AC toxins (Gille et al., 2004, 2005; Mou et al., 2006; Göttle et al., 2007, 2009; Taha et al., 2009). Like mAC and CyaA, edema factor AC toxin from *Bacillus anthracis* shows activation-dependent fluorescence increases with MANT-nucleotides (Taha et al., 2009). However, the affinity of edema factor for TNP-nucleotides is too low to allow for the conduction of fluorescence studies (data not shown).

Future Development of mAC Inhibitors. The development of isoform-selective AC inhibitors is an important and ambitious long-term goal. In particular, ACV inhibitors are promising drug candidates for the treatment of heart failure and ageing-related diseases (Iwatsubo et al., 2004; Rottlaender et al., 2007; Yan et al., 2007; Göttle et al., 2009). The identification of TNP-nucleotides as holo-AC inhibitors is an important step toward the achievement of this goal since TNP-nucleotides surpass the corresponding MANT-nucleotides in terms of potency at ACV by up to 50-fold (Table 3) (Gille et al., 2004; Göttle et al., 2009). MANT-inosine 5′-triphosphate is the most potent ACV inhibitor known so far (K_i, 1 nM) (Göttle et al., 2009). Thus, we predict that TNP-inosine 5′-triphosphate, which is not available to us at the present time, will be an even more potent ACV inhibitor. Whereas TNP-nucleotides do not surpass MANT-nucleotides in terms of AC isoform selectivity, the 2′,3′-*O*-ribosyl substitution with a phenyl ring offers numerous opportunities for chemical modifications. Specifically, some of the nitro groups attached to the phenyl ring could be deleted or exchanged against other functional groups. Given the conformational flexibility of the catalytic site of mACs together with the fact that the inhibition profiles of various mACs are not identical, the systematic analysis of the structure/activity relationships of phenyl ring substitutions combined with molecular modeling studies may ultimately yield AC isoform-selective inhibitors.

In a previous study, we showed that MANT-GDP and MANT-ADP are phosphorylated to MANT-GTP and MANT-ATP, respectively, by the NTP-regenerating system consisting of mono(cyclohexyl)ammonium phosphoenol pyruvate, pyruvate kinase, and myokinase (Gille et al., 2004). Likewise, the NTP-regenerating system increased the inhibitory potencies of TNP-AMP and TNP-ADP to the values of TNP-ATP using ACV as model AC (data not shown). These data show that TNP-AMP and TNP-ADP can be readily phosphorylated. This is an important property for intact cell experiments with lipophilic pronucleotide inhibitors that have to be converted to the actual inhibitory compounds (Laux et al., 2004). Thus, the present study provides an important starting point for the development of potent and selective mAC and sGC inhibitors.

Acknowledgments

We thank S. Brüggemann and A. Seefeld for expert technical assistance and the reviewers for constructive critique.

References

Ahuja N, Kumar P, and Bhatnagar R (2004) The adenylate cyclase toxins. *Crit Rev Microbiol* **30:**187–196.

Chen Y, Cann MJ, Litvin TN, Iourgenko V, Sinclair ML, Levin LR, and Buck J (2000) Soluble adenylyl cyclase as an evolutionarily conserved bicarbonate sensor. *Science* **289:**625–628.

Defer N, Best-Belpomme M, and Hanoune J (2000) Tissue specificity and physiological relevance of various isoforms of adenylyl cyclase. *Am J Physiol Renal Physiol* **279:**F400–F416.

Derbyshire ER and Marletta MA (2009) Biochemistry of soluble guanylate cyclase. *Handb Exp Pharmacol* **191:**17–31.

Gille A, Guo J, Mou TC, Doughty MB, Lushington GH, and Seifert R (2005) Differential interactions of G-proteins and adenylyl cyclase with nucleoside 5′-triphosphates, nucleoside 5′-[γ-thio]triphosphates and nucleoside 5′-[β,γ-imido]triphosphates. *Biochem Pharmacol* **71:**89–97.

Gille A, Liu HY, Sprang SR, and Seifert R (2002) Distinct interactions of GTP, UTP, and CTP with G_s proteins. *J Biol Chem* **277:**34434–34442.

Gille A, Lushington GH, Mou TC, Doughty MB, Johnson RA, and Seifert R (2004) Differential inhibition of adenylyl cyclase isoforms and soluble guanylyl cyclase by purine and pyrimidine nucleotides. *J Biol Chem* **279:**19955–19969.

Gille A and Seifert R (2003a) 2′(3′)-*O*-(*N*-Methylanthraniloyl)-substituted GTP analogs: a novel class of potent competitive adenylyl cyclase inhibitors. *J Biol Chem* **278:**12672–12679.

Gille A and Seifert R (2003b) Low-affinity interactions of BODIPY-FL-GTPγS and BODIPY-FL-GppNHp with G_i- and G_s-proteins. *Naunyn Schmiedebergs Arch Pharmacol* **368:**210–215.

Göttle M, Dove S, Steindel P, Shen Y, Tang WJ, Geduhn J, König B, and Seifert R (2007) Molecular analysis of the interaction of *Bordetella pertussis* adenylyl cyclase with fluorescent nucleotides. *Mol Pharmacol* **72:**526–535.

Göttle M, Geduhn J, König B, Gille A, Höcherl K, and Seifert R (2009) Characterization of mouse heart adenylyl cyclase. *J Pharmacol Exp Ther* **329:**1156–1165.

Hiratsuka T (2003) Fluorescent and colored trinitrophenylated analogs of ATP and GTP. *Eur J Biochem* **270:**3479–3485.

Hiratsuka T (1983) New ribose-modified fluorescent analogs of adenine and guanine nucleotides available as substrates for various enzymes. *Biochim Biophys Acta* **742:**496–508.

Iwatsubo K, Minamisawa S, Tsunematsu T, Nakagome M, Toya Y, Tomlinson JE, Umemura S, Scarborough RM, Levy DE, and Ishikawa Y (2004) Direct inhibition of type 5 adenylyl cyclase prevents myocardial apoptosis without functional deterioration. *J Biol Chem* **279:**40938–40945.

Jameson DM and Eccleston JF (1997) Fluorescent nucleotide analogs: synthesis and applications. *Methods Enzymol* **278:**363–390.

Koesling D, Russwurm M, Mergia E, Mullershausen F, and Friebe A (2004) Nitric oxide-sensitive guanylyl cyclase: structure and regulation. *Neurochem Int* **45:**813–819.

Laux WH, Pande P, Shoshani I, Gao J, Boudou-Vivet V, Gosselin G, and Johnson RA (2004) Pro-nucleotide inhibitors of adenylyl cyclase in intact cells. *J Biol Chem* **279:**13317–13332.

Liu HY, Wenzel-Seifert K, and Seifert R (2001) The olfactory G protein $G_{\alpha olf}$ possesses lower GDP-affinity and deactivates more rapidly than $G_{s\alpha S}$: consequences for receptor-coupling and adenylyl cyclase activation. *J Neurochem* **78:**325–338.

Mou TC, Gille A, Fancy DA, Seifert R, and Sprang SR (2005) Structural basis for the inhibition of mammalian membrane adenylyl cyclase by 2′(3′)-*O*-(N-methylanthraniloyl)-guanosine 5′-triphosphate. *J Biol Chem* **280:**7253–7261.

Mou TC, Gille A, Suryanarayana S, Richter M, Seifert R, and Sprang SR (2006) Broad specificity of mammalian adenylyl cyclase for interaction with 2′,3′-substituted purine- and pyrimidine nucleotide inhibitors. *Mol Pharmacol* **70:**878–886.

Newton RP, Kingston EE, Hakeem NA, Salih SG, Beynon JH, and Moyse CD (1986) Extraction, purification, identification and metabolism of 3′,5′-cyclic UMP, 3′,5′-cyclic IMP and 3′,5′-cyclic dTMP from rat tissues. *Biochem J* **236:**431–439.

Newton RP, Salih SG, Salvage BJ, and Kingston EE (1984) Extraction, purification and identification of cytidine 3′,5′-cyclic monophosphate from rat tissues. *Biochem J* **221:**665–673.

Newton RP, Salvage BJ, and Hakeem NA (1990) Cytidylate cyclase: development of assay and determination of kinetic properties of a cytidine 3′,5′-cyclic monophosphate-synthesizing enzyme. *Biochem J* **265:**581–586.

Pinto C, Hübner M, Gille A, Richter M, Mou TC, Sprang SR, and Seifert R (2009) Differential interactions of the catalytic subunits of adenylyl cyclase with forskolin analogs. *Biochem Pharmacol* **78:**62–69.

Pinto C, Papa D, Hübner M, Mou TC, Lushington GH, and Seifert R (2008) Activation and inhibition of adenylyl cyclase isoforms by forskolin analogs. *J Pharmacol Exp Ther* **325:**27–36.

Rottlaender D, Matthes J, Vatner SF, Seifert R, and Herzig S (2007) Functional adenylyl cyclase inhibition in murine cardiomyocytes by 2′(3′)-*O*-(*N*-methylanthraniloyl)-guanosine 5′-[γ-thio]triphosphate. *J Pharmacol Exp Ther* **321:**608–615.

Schlicker C, Rauch A, Hess KC, Kachholz B, Levin LR, Buck J, and Steegborn C (2008) Structure-based development of novel adenylyl cyclase inhibitors. *J Med Chem* **51:**4456–4464.

Schmidt HH, Schmidt PM, and Stasch JP (2009) NO- and haem-independent soluble guanylate cyclase activators. *Handb Exp Pharmacol* **191:**309–339.

Seifert R, Gether U, Wenzel-Seifert K, and Kobilka BK (1999) Effects of guanine, inosine, and xanthine nucleotides on β_2-adrenergic receptor/G_s interactions: evidence for multiple receptor conformations. *Mol Pharmacol* **56:**348–358.

Seifert R, Wenzel-Seifert K, Lee TW, Gether U, Sanders-Bush E, and Kobilka BK (1998) Different effects of $G_{s\alpha}$ splice variants on β_2-adrenoceptor-mediated signaling. The β_2-adrenoceptor coupled to the long splice variant of $G_{s\alpha}$ has properties of a constitutively active receptor. *J Biol Chem* **273:**5109–5116.

Sunahara RK, Beuve A, Tesmer JJ, Sprang SR, Garbers DL, and Gilman AG (1998) Exchange of substrate and inhibitor specificities between adenylyl and guanylyl cyclases. *J Biol Chem* **273:**16332–16338.

Sunahara RK and Taussig R (2002) Isoforms of mammalian adenylyl cyclase. Multiplicities of signaling. *Mol Interv* **2:**168–184.

Taha HM, Schmidt J, Göttle M, Suryanarayana S, Shen Y, Tang WJ, Gille A, Geduhn J, König B, Dove S, et al. (2009) Molecular analysis of the interaction of anthrax adenylyl cyclase toxin, edema factor, with 2′(3′)-*O*-(*N*-(methyl)anthraniloyl)-substituted purine and pyrimidine nucleotides. *Mol Pharmacol* **75:**693–703.

Tesmer JJ, Dessauer CW, Sunahara RK, Murray LD, Johnson RA, Gilman AG, and Sprang SR (2000) Molecular basis for P-site inhibition of adenylyl cyclase. *Biochemistry* **39:**14464–14471.

Tesmer JJ, Sunahara RK, Fancy DA, Gilman AG, and Sprang SR (2002) Crystallization of complex between soluble domains of adenylyl cyclase and activated $G_{s\alpha}$. *Methods Enzymol* **345:**198–206.

Tesmer JJ, Sunahara RK, Gilman AG, and Sprang SR (1997) Crystal structure of the catalytic domains of adenylyl cyclase in a complex with $G_{s\alpha\text{-}GTP\gamma S}$. *Science* **278:**1907–1916.

Wenzel-Seifert K, Arthur JM, Liu HY, and Seifert R (1999) Quantitative analysis of formyl peptide receptor coupling to $G_i\alpha_1$, $G_i\alpha_2$, and $G_i\alpha_3$. *J Biol Chem* **274:**33259–33266.

Yan L, Vatner DE, O'Connor JP, Ivessa A, Ge H, Chen W, Hirotani S, Ishikawa Y, Sadoshima J, and Vatner SF (2007) Type 5 adenylyl cyclase disruption increases longevity and protects against stress. *Cell* **130:**247–258.

Address correspondence to: Dr. Roland Seifert, Institute of Pharmacology, Medical School of Hannover, Carl-Neuberg-Str. 1, D-30625 Hannover, Germany. E-mail: seifert.roland@mh-hannover.de